Full dimensional (15 dimensional) quantum-dynamical simulation of the protonated water-dimer IV: Isotope effects in the infrared spectra of D(D2O)2+, H(D2O)2+, and D(H2O)2+ isotopologues.

Oriol Vendrell, Fabien Gatti, Hans-Dieter Meyer

Full dimensional (15 dimensional) quantum-dynamical simulation of the protonated water-dimer IV: Isotope effects in the infrared spectra of $D(D_2O)_2^+$, $H(D_2O)_2^+$, and $D(H_2O)_2^+$ isotopologues

Oriol Vendrell,[1,a)] Fabien Gatti,[2,b)] and Hans-Dieter Meyer[1,c)]
[1]*Theoretische Chemie, Physikalisch-Chemisches Institut, Universität Heidelberg, INF 229, D-69120 Heidelberg, Germany*
[2]*CTMM, Institut Charles Gerhardt (UMR 5232-CNRS), CC 1501, Université de Montpellier II, F-34095 Montpellier, Cedex 05, France*

(Received 26 May 2009; accepted 30 June 2009; published online 17 July 2009)

The infrared spectra of $H(H_2O)_2^+$, $D(D_2O)_2^+$, $H(D_2O)_2^+$, and $D(H_2O)_2^+$ isotopologues of the Zundel cation in the spectral range of 0–4000 cm^{-1} are computed by quantum dynamics in full dimensionality using the multiconfiguration time-dependent Hartree method. The spectra present dramatic isotope effects in the middle spectral region between 600 and 2000 cm^{-1}. Not only the expected line shifts due to isotopic substitution take place but the intensities of the peaks and the number of absorptions with appreciable intensity vary. The most complex spectrum is the one of $H(D_2O)_2^+$, in which a group of at least four coupled vibrational modes is found in a narrow spectral range between 1000 and 1500 cm^{-1} and is responsible for the three peaks found in this spectral region. The simplest spectrum of the series corresponds to $D(H_2O)_2^+$. In this case deuteration of the central position induces decoupling of the vibrational modes, especially of the asymmetric central proton mode and the *ungerade* water bending, leading to a spectrum which is easy to assign and interpret. Zero-point energies and low energy vibrational eigenstates of each isotopologue related to the wagging (pyramidalization) and water-water internal relative rotation are computed using the block improved relaxation algorithm. The effect of isotopic substitution on these states is discussed. The reported simulations provide detailed information on the dynamics and vibrational spectroscopy of the Zundel cation and contribute to our general understanding of protonated water clusters and the hydrated proton. © *2009 American Institute of Physics*. [DOI: 10.1063/1.3183166]

I. INTRODUCTION

The scientific interest in protonated water clusters and proton transport has gained considerable momentum over the last years.[1,2] Hydrated protons mediate charge transport in biological environment[3,4] and in bulk water,[5–7] and linear chains of water molecules have been found to exhibit high proton mobilities.[8–10] Protonated water clusters are often found embedded in complex environments. Owing to the development of infrared (IR) laser techniques during the last decade, the vibrational dynamics of isolated clusters of diverse size and shape can nowadays be experimentally studied.[2,11] Accurate IR spectra measured for these systems unravel intimate details of their complex dynamics. Assignment and interpretation of these IR spectra require sophisticated theoretical approaches owing to the soft, anharmonic, and coupled interatomic potential featured by the clusters. Unfortunately, accurate quantum-dynamical calculations of such spectra are still beyond reach for all but the smallest clusters.

The protonated water dimer, also known as Zundel cation, is the smallest protonated water cluster in which a proton is shared between different water molecules. This system has been the subject of intense experimental[12–17] and theoretical[15–30] investigations during the last years. The IR spectrum of $H(H_2O)_2^+$ was measured in the gas phase by multiphoton IR techniques using free electron lasers[12,13] and later by messenger atom IR spectroscopy.[14,15] The spectra measured using Ne as the messenger atom were found to be very similar to accurate theoretical spectra obtained with the multiconfiguration time-dependent Hartree (MCTDH) method.[24,26] MCTDH calculations of the IR spectrum of $H(H_2O)_2^+$ completely reproduced and, most importantly, explained various features of IR spectrum which had remained elusive due to the strongly coupled dynamics of the cation.[24,26]

IR spectra of various isotopologues of the Zundel cation, namely, $D(D_2O)_2^+$ and $H(D_2O)_2^+$, were recently measured using Ar as the tagging atom.[16] These spectra presented large differences in position and intensity of the spectral lines with respect to the spectrum of $H(H_2O)_2^+$, which were beyond the expected line shifts due to deuteration. The spectra of the $D(D_2O)_2^+$, $H(D_2O)_2^+$, and $D(H_2O)_2^+$ isotopologues were recently computed by Vendrell *et al.*[28] using MCTDH and the most important assignments were briefly discussed. The computed spectra were in good agreement with the experimental Ar-tagging spectra, although the experimental spectra present relatively broad features due to interaction of the tagging atom with the Zundel cation. Unfortunately, Ne-

[a)]Electronic mail: oriol.vendrell@pci.uni-heidelberg.de.
[b)]Electronic mail: gatti@univ-montp2.fr.
[c)]Electronic mail: hans-dieter.meyer@pci.uni-heidelberg.de.

tagged messenger IR spectra of isotopically substituted forms of the Zundel cation, which would be expected to have a better resolution with narrower peaks, have not yet been measured.

In this paper we compute, assign, and explain the IR spectra of the $D(D_2O)_2^+$, $H(D_2O)_2^+$, and $D(H_2O)_2^+$ isotopologues using the MCTDH method. The IR spectrum of $H(H_2O)_2^+$ is also described here, since it serves as a reference to discuss the other spectra. The dramatic differences between these spectra are explained by underlying couplings between vibrational modes, which are strongly mass dependent in such a way that different couplings and Fermi resonances between bright and dark states become active or inactive depending on the isotopic substitution of the cluster. We also compute the zero-point energy (ZPE) and various low lying excited states and their energies by block improved relaxation (BIR). These low frequency states are mostly related to the wagging (pyramidalization) and water-water relative rotation coordinates. The tunneling splitting due to the barrier along the relative water-water internal rotation is also computed for $D(D_2O)_2^+$ and compared to the value for $H(H_2O)_2^+$.

The paper is organized as follows. Section II gives some remarks on the theory and methods used for the computations. Section III A describes the calculation of the ZPE and several vibrational eigenstates for each isotopologue. Section III B discusses the calculation and assignment of the IR spectra and Sec. IV concludes and gives some outlook.

II. THEORY AND METHODS

All reported quantum-dynamical calculations are performed by the MCTDH method[31–33] using the Heidelberg MCTDH package of programs.[34] The configuration of the Zundel cation is given by a set of curvilinear coordinates, which is crucial for the description of the large amplitude motions and anharmonicities featured by the cluster.[24–26,29] A detailed discussion of the 15 internal coordinates describing the system and the derivation of the corresponding kinetic energy operator (KEO) is given in Refs. 25 and 29. The 15 internal coordinates are briefly reintroduced here to make this presentation self-contained. These are the distance between the oxygen atoms of both water molecules (R), the position of the central proton with respect to the center of mass of the oxygen atoms (x,y,z), and the Euler angles defining the relative orientation between the two water molecules, namely, waggings: (γ_A,γ_B), rockings: (β_A,β_B), and internal relative rotation of one water with respect to the other: (α) and the Jacobi coordinates account for the particular configuration of each water molecule $(R_{1(A,B)},R_{2(A,B)},\theta_{(A,B)})$, where R_{1x} is the distance between the oxygen atom and the center of mass of the corresponding H_2 fragment, R_{2x} is the H–H distance, and θ_x is the angle between these two vectors. All calculations in this work are based on the D_{2d} setup introduced in Ref. 29. Only the splitting due to the barrier along the internal water-water rotation coordinate is computed in G_{16}.[29] The set of coordinates employed can describe isotopic substitutions in which the masses of both hydrogens of each water molecule are equal.

TABLE I. Zero-point energies of the isotopologues $H(H_2O)_2^+$, $D(H_2O)_2^+$, $H(D_2O)_2^+$, and $D(D_2O)_2^+$. DMC energies of Refs. 16 and 21, MCTDH energies computed with a (12,22,22,16,10,10) SPF basis, and MCTDH-DMC energy difference.

	DMC	MCTDH	Difference
$H(H_2O)_2^+$	12 393	12 398.8	5.84
$D(H_2O)_2^+$	11 837	11 846.8	9.82
$H(D_2O)_2^+$	9706	9710.7	4.71
$D(D_2O)_2^+$	9143	9143.0	−0.05

The consideration of asymmetric isotopic substitutions in the water molecules modifies the water Jacobi coordinates as the H–D center of mass differs from the H_2 one. This introduces new coupling terms in the KEO and would require a recomputation of the clusters of the n-mode representation in the new coordinates.

To account for the interatomic potential we make use of the potential energy surface (PES) of Bowman and co-workers,[20] which constitutes the most accurate *ab initio* surface available to date for this system. The PES expansion used in this work has been presented and discussed in detail in Ref. 29. The potential energy operator is constructed as an n-mode representation,[35,36] also referred to as cut high dimensional model representation (HDMR),[37] which is adapted to take advantage of mode combination in the MCTDH wave function.[25] The number of configurations of the MCTDH expansion is drastically reduced by using mode combination, i.e., combining physical coordinates into logical coordinates. The 15 degrees of freedom are combined into six logical coordinates Q_i according to the following combination scheme: $Q_1=[z,R]$, $Q_2=[\alpha,x,y]$, $Q_3=[\gamma_A,\gamma_B]$, $Q_4=[\beta_A,\beta_B]$, $Q_5=[R_{1A},R_{2A},\theta_{1A}]$, and $Q_6=[R_{1B},R_{2B},\theta_{1B}]$. n-mode potentials of second and third order in the logical coordinates are transformed to product form by employing the potfit algorithm.[38,39]

The MCTDH wave function reads

$$\Psi(Q_1,\ldots,Q_6,t)=\sum_{j_1}^{n_1}\cdots\sum_{j_6}^{n_6}A_{j_1,\ldots,j_6}(t)\prod_{\kappa=1}^{6}\varphi_{j_\kappa}^{(\kappa)}(Q_\kappa,t). \quad (1)$$

In several places we specify the size of the single particle function (SPF) basis used for a particular calculation as $(n_1,n_2,n_3,n_4,n_5,n_6)$, where n_κ is the number of SPFs for combined mode Q_κ, and the number of configurations is simply $\Pi_{\kappa=1}^{6}n_\kappa$. Further details on the mode combination scheme used in this work are given in Ref. 29.

III. RESULTS AND DISCUSSION

A. Zero point energies and vibrationally excited states

The ZPE of the four considered isotopologues is given in Table I. The MCTDH values were computed by *improved* relaxation[40,41] using a (12,22,22,16,10,10) SPF basis. The MCTDH values are given as differences to the corresponding diffusion Monte Carlo (DMC) energies computed by McCoy and co-workers,[16] which are taken as a reference. In Ref. 29 a convergence study of the ZPE of $H(H_2O)_2^+$ was carried out.

TABLE II. For each isotopologue, vibrational eigenenergies in the lowest frequency region computed with the BIR algorithm. The calculations were performed with a (12,26,16,12,8,8) SPF basis.

	$H(H_2O)_2^+$	$D(H_2O)_2^+$	$H(D_2O)_2^+$	$D(D_2O)_2^+$
$\|\Psi_{w_{1a}}\rangle$	102.2	98.7	51.5	49.2
$\|\Psi_{w_{1b}}\rangle$	102.2	99.3	52.2	50.0
$\|\Psi_{1\alpha}\rangle$	152.8	152.6	97.2	94.9
$\|\Psi_{w_2}\rangle$	231.2	226.5	134.9	134.0
$\|\Psi_{w_{1a},1\alpha}\rangle$	255.9	253.4	162.4	161.2
$\|\Psi_{w_{1b},1\alpha}\rangle$	255.9	253.7	162.8	161.6
$\|\Psi_{w_{2},1\alpha}\rangle$	379.1	377.0	250.9	250.8
$\|\Psi_{w_3}\rangle$	386.3	372.2	254.9	247.1
$\|\Psi_{w_4}\rangle$	447.0	444.4	303.9	304.4

The largest calculation used a (14,30,30,20,10,10) SPF basis, which corresponds to 25 200 000 configurations, yielding (within D_{2d}) a ZPE of 5.4 cm^{-1} above the DMC value. The MCTDH value obtained with this (14,30,30,20,10,10) SPF basis is expected to be converged to better than 1 cm^{-1} with respect to the true variational energy on the n-mode representation of the potential.[29] That value lies only 0.4 cm^{-1} below the one obtained with a (12,22,22,16,10,10) SPF basis in this work. As the MCTDH energies are variational, i.e., they are upper bounds to the ZPE of the potential model used,[29] we assume that the MCTDH values reported here for the four isotopologues lie between 1 and 2 cm^{-1} above the ZPE of our potential model. The error introduced by the n-mode representation of the potential is rather uncontrolled, but we have made a careful statistical analysis of this error and have shown that the potential model used is reliable.[29] Although we use the same potential model for all four isotopologues, the error introduced in the ZPE will depend on the specific isotopologue because the different wave functions weight different areas of the potential differently. However, this effect is assumed to be small and one expects the ZPE error introduced by the potential model to be similar for all four isotopologues. These arguments make the rather erratic behavior of the differences between MCTDH and DMC energies (see Table I) somewhat surprising. However, DMC has statistical rather than systematic errors and the data of Table I indicate that the estimated DMC statistical error of ± 5 cm^{-1} is realistic.

Table II reports the energies of several low-lying vibrationally excited states of the four isotopologues computed by BIR.[40,41] Excited state energies are given relative to the ground vibrational-state energy. The calculations were performed with a (12,26,16,12,8,8) SPF basis and ten states were simultaneously calculated, resulting in a vector of coefficients of length 38 338 560. The results for $H(H_2O)_2^+$, which correspond to the D_{2d} setup, were already reported in Ref. 29. There it was shown that the agreement with energies computed within G_{16} is excellent. Vibrationally excited states are given names as $(n_1X_1,n_2X_2,\ldots)$, where n_i designates the quanta of excitation in coordinate X_i, while all other coordinates remain unexcited in a separable limit. Excitations not designated according to this convention are defined when first introduced.

The two water molecules in the Zundel cation can rotate with respect to each other. This motion is described by the periodic coordinate α. The barrier along α is centered at 0° and 180° and gives rise to a tunneling splitting, which, for $H(H_2O)_2^+$, has been computed to be 1 cm^{-1}.[26,29] The calculation of the tunneling splitting caused by the barrier along α needs to be computed within G_{16} symmetry, in which α is defined in the range $[0,2\pi)$.[29] The tunneling splitting for $D(D_2O)_2^+$ has been computed with a BIR calculation of the ground and first vibrational excited states and has been found to be of only 0.06 cm^{-1}.

All calculations of excited vibrational states and spectra that follow have been performed within the D_{2d} setup, in which the α coordinate spans the region $(0,\pi)$.[29] As this has been found to be an excellent approximation for $H(H_2O)_2^+$, it supposes an even better approximation for isotopologues with terminal hydrogens substituted by deuterium. The low energy region contains excitations related to the wagging coordinates γ_A,γ_B and to the internal rotation coordinate α. The $(w_{1a,b})$ excitation corresponds to a doubly degenerated one-quantum excitation of the wagging coordinates. In *ket* notation the two degenerate states are given by $(|01\rangle \pm |10\rangle)/\sqrt{2}$, where each entry represents the quanta of excitation in the wagging coordinate of each water molecule. Wagging excitations (w_2), (w_3), and (w_4) correspond to two-quanta excitations, and in *ket* notation are given as[26]

$$(w_2) \equiv |11\rangle, \tag{2a}$$

$$(w_3) \equiv (|20\rangle - |02\rangle)/\sqrt{2}, \tag{2b}$$

$$(w_4) \equiv (|20\rangle + |02\rangle)/\sqrt{2}. \tag{2c}$$

Comparison of the excitation energies along $H(H_2O)_2^+$ and $D(H_2O)_2^+$ columns of Table II on the one side and along $H(D_2O)_2^+$ and $D(D_2O)_2^+$ columns on the other side shows that states with the same excitation character have energies that differ in almost all cases by less than 5 cm^{-1}. This indicates that wagging and α excitations are well decoupled from the central proton motion and depend only on the isotopic substitution of the external positions. An exception to this is the (w_3) excited state, which presents slightly larger differences within each pair of isotopologues that share the same isotopic substitution in external positions. The (w_3) energy in $H(H_2O)_2^+$ is 14 cm^{-1} larger than in $D(H_2O)_2^+$, and the (w_3) energy in $H(D_2O)_2^+$ is 7 cm^{-1} larger than in $D(D_2O)_2^+$. The (w_3) state corresponds to the excitation in which one water is found in a planar configuration while the other one is pyramidalized and vice versa. This state has the correct symmetry to couple to the $(1z)$ central proton excitation.[24,26] The variations in energy of this state within each pair of isotopologues indicate that a certain coupling to the central proton motion exists for (w_3). The (w_3) state does not present appreciable IR intensity in any of the computed IR spectra discussed in Sec. III B. However, it will be shown below that states corresponding to combinations of (w_3) with a single or double excitation of coordinate R can borrow intensity from bright states through Fermi resonances.

B. IR spectra of $D(H_2O)_2^+$, $H(D_2O)_2^+$, and $D(D_2O)_2^+$

The IR spectrum is computed as discussed in Refs. 26 and 29 by Fourier transform of the autocorrelation function of the dipole-operated ground state. The IR spectrum of $H(H_2O)_2^+$ in the full range of 0–4000 cm^{-1} was recently computed and analyzed by Vendrell *et al.*[24,26,29] using the MCTDH method. The assignments of all bright lines of the spectrum were reported in Ref. 26. The IR spectrum of the nondeuterated form $H(H_2O)_2^+$ was recently revisited[29] and computed using the same coordinates and potential energy expansion as used in this work for the $D(D_2O)_2^+$, $H(D_2O)_2^+$, and $D(H_2O)_2^+$ isotopologues. A (11,12,12,11,7,7) SPF basis provided converged spectra for $H(H_2O)_2^+$ and it is the basis used here for the calculation of the IR spectra of the isotopically substituted cations. A less detailed discussion on the spectra of the isotopically substituted forms of the Zundel cation was recently given by Vendrell *et al.*[28] There a smaller (10,10,10,10,6,6) SPF basis was used.

Figure 1 presents the computed spectra for $H(H_2O)_2^+$, $D(H_2O)_2^+$, $H(D_2O)_2^+$, and $D(D_2O)_2^+$. The interpretation of the IR spectra in Fig. 1 requires definite assignments of the spectral lines and an understanding of their origin. Zeroth-order states are used as a tool to perform such assignments. They correspond to well defined local excitations of the system, e.g., the bending mode of the water molecules or the one-quantum excitation of the proton-transfer mode, and they are usually constructed as products of eigenfunctions of low dimensional mode Hamiltonians, each of them defined in the space of one of the combined coordinates. A more specific definition and procedures to obtain them in the context of MCTDH were presented elsewhere.[26] In the following, $|\Phi_l\rangle$ refers to the vibrational wave function of a zeroth-order state while $|\Psi_m\rangle$ corresponds to a vibrational eigenstate. The quantities used for assignments are the $|\langle\Phi_l|\Psi_m\rangle|^2$ products, which tell to which extent a particular and well defined zeroth-order vibration participates in a certain spectral line. The overlaps are obtained in the time representation via the formula[40]

$$|\langle\Phi_l|\Psi_m\rangle|^2 = \frac{\pi}{2T}\mathrm{Re}\int_0^T e^{iE_m t/\hbar}\langle\Phi_l|e^{-iHt/\hbar}|\Phi_l\rangle\cos\left(\frac{\pi t}{2T}\right)dt. \tag{3}$$

Even though each spectral line contains contributions from all or some of the considered zeroth-order states (nonvanishing $|\langle\Phi_l|\Psi_m\rangle|^2$ elements), there is usually a zeroth-order state that contributes to a specific transition appreciably more than the others. Thus, when we refer to a certain spectral line as the (*laboratory*) transition or to the corresponding eigenstate as $|\Psi_{\mathrm{lab}}\rangle$, it is because it is possible to identify the zeroth-order state $|\Phi_{\mathrm{lab}}\rangle$ as the *leading* contribution to $|\Psi_{\mathrm{lab}}\rangle$. As a side remark, although it was not explicitly mentioned there, the same principle applies in order to assign labels to the eigenstates in Table II. In the case of large couplings it may not be possible to cleanly disentangle the spectrum into one-to-one assignments of spectral peaks to zeroth-order states, since a given transition may present similar contributions from two or more zeroth-order states.

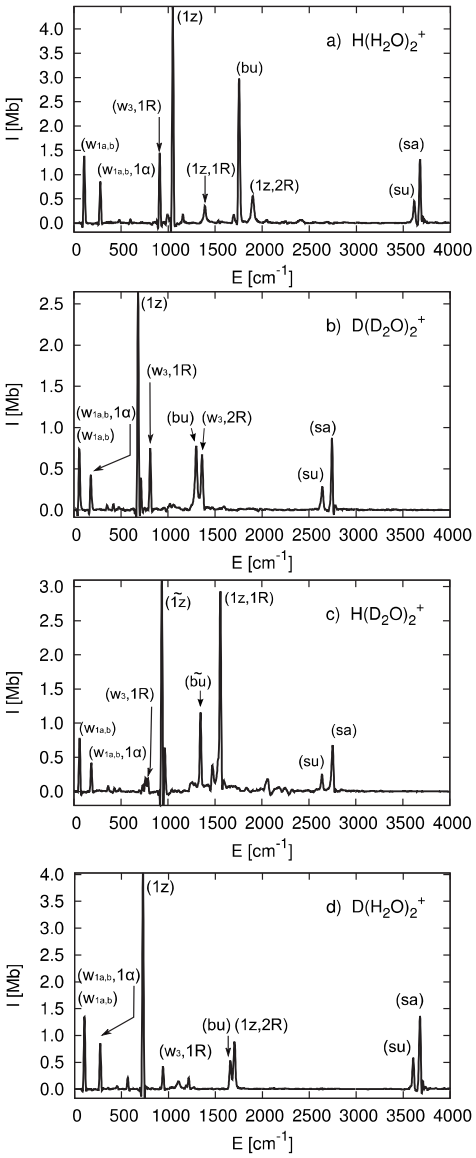

FIG. 1. Computed IR spectra of the (a) $H(H_2O)_2^+$, (b) $D(D_2O)_2^+$, (c) $H(D_2O)_2^+$, and (d) $D(H_2O)_2^+$ isotopologues of the Zundel cation with assignments of the most important peaks.

The lowest frequency region of the four spectra in Fig. 1 presents two lines. From low to high energy they correspond to a doubly degenerate one-quantum excitation of the wagging modes $(w_{1a,b})$ and its combination with a one-quantum excitation of the internal rotation of one water molecule with respect to the other $(w_{1a,b},1\alpha)$, respectively. In the highest energy region of the four spectra in Fig. 1 two peaks related to the O–H stretching modes are found. There are three O–H stretching states which can be represented in *ket* notation as

$$(sg) \equiv (|10,00\rangle + |01,00\rangle + |00,10\rangle + |00,01\rangle)/2, \tag{4a}$$

$$(su) \equiv (|10,00\rangle + |01,00\rangle - |00,10\rangle - |00,01\rangle)/2, \tag{4b}$$

$$(sa) \equiv ((|10,00\rangle - |01,00\rangle) \pm (|00,10\rangle - |00,01\rangle))/2. \tag{4c}$$

The first two entries in each *ket* provide the quanta of excitation in each O–H bond of one of the water molecules,

TABLE III. For each isotopologue, vibrational energies of various eigenstates in the middle and high frequency regions. The energies were obtained by Fourier analysis of the autocorrelation function of propagated wave packets corresponding to either the dipole-operated ground state or zeroth-order states. As discussed in the text, the naming of eigenstates $|\Psi_{1z}\rangle$ and $|\Psi_{bu}\rangle$ in the $H(D_2O)_2^+$ case is a bit arbitrary due to the strong mixing of the underlying zeroth-order states.

	$H(H_2O)_2^+$	$D(H_2O)_2^+$	$H(D_2O)_2^+$	$D(D_2O)_2^+$
$\|\Psi_{w_3,1R}\rangle$	913.0	942.6	760.0	812.8
$\|\Psi_{1z}\rangle$	1050.1	728.9	936.0	683.1
$\|\Psi_{1z,1R}\rangle$	1392.0	1215.3	1558.6	1146.2
$\|\Psi_{w_3,2R}\rangle$	1560.0	1486.0	1245.7	1363.2
$\|\Psi_{bu}\rangle$	1756.3	1660.1	1346.7	1301.4
$\|\Psi_{1z,2R}\rangle$	1902.6	1703.8	2055.9	1615.2
$\|\Psi_{su}\rangle$	3617.8	3607.4	2640.4	2643.1
$\|\Psi_{sa}\rangle$	3679.8	3679.3	2753.9	2746.0

while the second two entries describe the quanta of excitation in each O–H bond of the other water molecule. The lowest frequency absorption in the high frequency domain corresponds to the symmetric *ungerade* stretching mode (*su*). Here symmetric/asymmetric refers to the symmetry of the motion within one water and gerade/ungerade to the symmetry between the two waters. The higher frequency line corresponds to the doubly degenerate *asymmetric* stretching mode (*sa*). The *gerade* stretching (*sg*) state is a dark state by symmetry. The relative position of the wagging and O–H stretching excitations does not change after deuteration. Only the expected redshifts take place for $H(D_2O)_2^+$ and $D(D_2O)_2^+$, that is, upon substitution of the terminal hydrogen atoms by deuterium.

The IR spectra of the four considered isotopologues strongly differ from each other in the middle spectral region between 600 and 2000 cm^{-1}. The assignment of the IR spectrum of $H(H_2O)_2^+$ in Fig. 1(a) has been already discussed by Vendrell *et al.*[24,26] They reintroduce here the most important elements of such spectrum since it serves as reference for the discussion of the other isotopologues. Table III contains eigenenergies of the middle and high frequency regions computed by Fourier analysis. For bright eigenstates the energies in Table III correspond to the positions of the peaks of the spectra in Fig. 1. Eigenenergies of states which are not bright or present very low intensity have been obtained by Fourier analysis of the autocorrelation function of propagated zeroth-order states. The computation of eigenstates by improved relaxation and BIR is restricted to the low energy region of the spectrum. In the middle and higher energy domains convergence to a particular eigenstate is very difficult due to the high density of states. Conversely, propagation is always possible, which enables the computation of eigenenergies by Fourier transform in these energy regions.

1. $H(H_2O)_2^+$

Figure 2 shows the IR spectrum of $H(H_2O)_2^+$ in the spectral region between 800 and 2000 cm^{-1} together with the experimental spectrum measured using Ar as the tagging agent.[14] As shown in Ref. 26 there is an excellent agreement between theory and Ne-tagging experiment. However, the

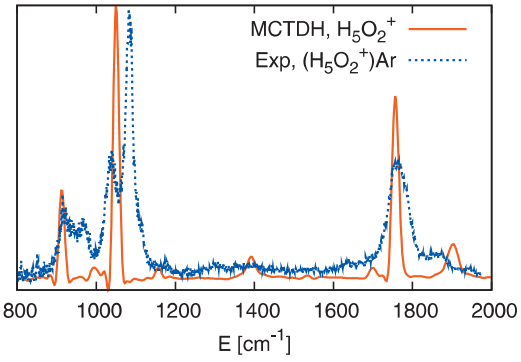

FIG. 2. For $H(H_2O)_2^+$ comparison of the computed MCTDH IR spectrum (full line) with an experimental spectrum measured using Ar as the messenger atom (dotted line) (Ref. 14).

spectrum measured using Ar presents broader lines and line doubling due to a stronger interaction of the Ar atom with the core cation. We show the Ar-tagged $H(H_2O)_2^+$ spectrum here to demonstrate the closeness of agreement between theory and Ar-tagged experiments one can expect. For the deuterated systems, unfortunately, there exist only spectra obtained with Ar tagging. The spectrum in Fig. 1(a) features five absorptions between 900 and 1900 cm^{-1} which can be assigned by resorting to five coupled zeroth-order states:[24,26] (1) $|\Phi_{w_3,1R}\rangle$, (2) $|\Phi_{1z}\rangle$, (3) $|\Phi_{1z,1R}\rangle$, (4) $|\Phi_{bu}\rangle$, and (5) $|\Phi_{1z,2R}\rangle$. Here (*bu*) indicates the ungerade water bending mode. The overlaps between zeroth-order states and eigenstates for $H(H_2O)_2^+$ are found in Table IV. These overlaps have smaller values as one might expect, and the numbers within one column do not add up to one. For such a strongly correlated system as the Zundel cation the definition of good zeroth-order states is difficult. The obvious choice used here, Hartree products of eigenfunctions of low-dimensional model Hamiltonians, depends on the precise definition of these model Hamiltonians. The numbers shown in Table IV hence may vary somewhat with the specific choice of the zeroth-order state, but the assignments of the correlated eigenstates are reliable.

The most intense line of the $H(H_2O)_2^+$ spectrum is related to the (1*z*) transition at 1050 cm^{-1} as the displacement of the proton along the O–O axis causes the largest variation in the dipole moment. Although the $|\Phi_{1z}\rangle$ zeroth-order state has a large contribution to the $|\Psi_{1z}\rangle$ eigenstate, the second most important contribution to $|\Psi_{1z}\rangle$ arises from $|\Phi_{1R,w_3}\rangle$, as seen in Table IV. The situation is reversed for the line centered at

TABLE IV. For $H(H_2O)_2^+$, matrix elements $|\langle\Phi_l|\Psi_m\rangle|^2$, where $|\Phi_l\rangle$ is a zeroth-order state and $|\Psi_m\rangle$ is an eigenstate. The naming of each eigenstate $|\Psi_m\rangle$ is based on the leading contribution of the zeroth-order states $|\Phi_l\rangle$.

$H(H_2O)_2^+$ Energy (cm^{-1})	$\|\Psi_{w_3,1R}\rangle$ 913	$\|\Psi_{1z}\rangle$ 1050	$\|\Psi_{1z,1R}\rangle$ 1392	$\|\Psi_{w_3,2R}\rangle$ 1560	$\|\Psi_{bu}\rangle$ 1756	$\|\Psi_{1z,2R}\rangle$ 1903
$\langle\Phi_{1R,w_3}\|$	0.61	0.19	0.00	0.00	0.02	0.00
$\langle\Phi_{1z}\|$	0.25	0.42	0.01	0.03	0.08	0.01
$\langle\Phi_{1z,1R}\|$	0.00	0.01	0.37	0.13	0.16	0.01
$\langle\Phi_{w_3,2R}\|$	0.00	0.00	0.33	0.33	0.02	0.01
$\langle\Phi_{bu}\|$	0.03	0.10	0.05	0.10	0.46	0.05
$\langle\Phi_{1z,2R}\|$	0.00	0.00	0.00	0.02	0.04	0.19

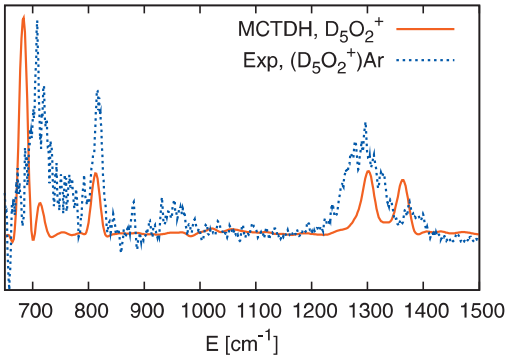

FIG. 3. For $D(D_2O)_2^+$ comparison of the computed MCTDH IR spectrum (full line) with an experimental spectrum measured using Ar as the messenger atom (dotted line) (Ref. 16).

913 cm^{-1}, in which the leading contribution is $|\Phi_{1R,w_3}\rangle$ and the second most important contribution is $|\Phi_{1z}\rangle$. Therefore the doublet of peaks centered at 1000 cm^{-1} in $H(H_2O)_2^+$ arises from a Fermi resonance between two strongly coupled zeroth-order states, $|\Phi_{1z}\rangle$ and $|\Phi_{1R,w_3}\rangle$. The next three lines of the spectrum correspond to the 1392 cm^{-1} $(1z,1R)$, 1756 cm^{-1} (bu), and 1903 cm^{-1} $(1z,2R)$ transitions, respectively. All three transitions, and specially (bu), have a nonnegligible contribution from the $|\Phi_{1z}\rangle$ zeroth-order state, from which they obtain a large part of their spectral intensity.[26] Moreover, the strong coupling between $|\Phi_{1z}\rangle$ and $|\Phi_{bu}\rangle$ modes is responsible for shifting the $(1z)$ and (bu) lines about 150 cm^{-1} down and up, respectively, with respect to their estimated uncoupled positions.[26,27] The eigenstate of energy 1392 cm^{-1} has, as already mentioned, $|\Phi_{1z,1R}\rangle$ as the leading contribution. However, the zeroth-order state $|\Phi_{w_3,2R}\rangle$ contributes appreciably to this eigenstate. Table IV has important nondiagonal contributions in the 2×2 upper-left corner, which are related to the Fermi resonance centered at 1000 cm^{-1}. Also the 3×3 block corresponding to $(1z,1R)$, $(w_3,2R)$, and (bu) denotes nonnegligible mixing of the zeroth-order states in the expansion of every one of the eigenstates.

2. $D(D_2O)_2^+$

Figure 3 presents the computed IR spectrum for $D(D_2O)_2^+$ together with the experimental spectrum measured using Ar as the tagging agent[16] in the spectral range between 650 and 1700 cm^{-1}. The two spectra agree well in the positions of the main features. The Ar spectrum presents quite broad features, which are a result of the interaction of the Ar atom with the cation. The MCTDH IR spectrum of $D(D_2O)_2^+$ is shown in Fig. 1(b) for the spectral range of 0–4000 cm^{-1}. The $(1z)$ peak is found here at 683 cm^{-1} and is, as in $H(H_2O)_2^+$, the most intense IR absorption. The $(w_3,1R)$ peak is found at 813 cm^{-1}. Therefore the characteristic doublet at about 1000 cm^{-1} in $H(H_2O)_2^+$ is also found in $D(D_2O)_2^+$, but with its constituent peaks in reverse order and shifted to lower frequencies. The (bu) peak is found at 1301 cm^{-1}, about 450 cm^{-1} below its position in $H(H_2O)_2^+$. $(1z,1R)$ appears in this case with a very low intensity, while $(1z,2R)$ does not appear at all in the spectrum of $D(D_2O)_2^+$. The position of these two eigenstates has been computed to be 1146 and 1615 cm^{-1}, respectively. Therefore they are located far from absorptions from which they could borrow intensity. Moreover, after deuteration the coupling between z and R is reduced since the system remains in deeper, less anharmonic regions of the potential, thus reducing even more the possibility for direct absorption of the $(1z,1R)$ and $(1z,2R)$ combinations. Close to the (bu) peak at 1301 cm^{-1} an absorption occurs at slightly higher frequency. This absorption was already found in the MCTDH IR spectrum of $D(D_2O)_2^+$ but had remained unassigned.[28] An absorption in this position is also seen as a shoulder to the (bu) peak in the experimental IR spectrum of $D(D_2O)_2^+$ (Ref. 16) in Fig. 3. The fact that this absorption is very close the (bu) peak immediately suggests that it may correspond to a Fermi resonance between two zeroth-order states. In fact, the analysis of propagated zeroth-order states using Eq. (3) reveals that this line has as the leading contribution the $(w_3,2R)$ excitation, as seen in Table V. Similarly as in $H(H_2O)_2^+$, $(1z,1R)$, $(w_3,2R)$, and (bu) zeroth-order states mix appreciably. However, in the IR spectrum of $D(D_2O)_2^+$ two peaks related to this group of three zeroth-order states have as leading contributions $(w_3,2R)$ and (bu) instead of $(1z,1R)$ and (bu) as in $H(H_2O)_2^+$. Table V presents the $|\langle\Phi_l|\Psi_m\rangle|^2$ matrix elements for the $D(D_2O)_2^+$ case. Similarly as in the $H(H_2O)_2^+$ case the matrix is diagonally dominant, which means that a leading contribution can be identified for each eigenstate. However, important nondiagonal elements are found in the 2×2 upper-left corner, which are indicative of a Fermi resonance between $|\Phi_{1R,w_3}\rangle$ and $|\Phi_{1z}\rangle$ zeroth-order states. The 3×3 block corresponding to $(1z,1R)$, (bu), and $(w_3,2R)$ has also nondiagonal elements, which are non-negligible. The small energy difference between (bu) and $(w_3,2R)$ results in this case in the Fermi resonance structure centered at 1330 cm^{-1}.

TABLE V. For $D(D_2O)_2^+$, matrix elements $|\langle\Phi_l|\Psi_m\rangle|^2$, where $|\Phi_l\rangle$ is a zeroth-order state and $|\Psi_m\rangle$ is an eigenstate. The naming of each eigenstate $|\Psi_m\rangle$ is based on the leading contribution of the zeroth-order states $|\Phi_l\rangle$.

$D(D_2O)_2^+$ Energy (cm^{-1})	$\|\Psi_{1z}\rangle$ 683	$\|\Psi_{w_3,1R}\rangle$ 813	$\|\Psi_{1z,1R}\rangle$ 1146	$\|\Psi_{bu}\rangle$ 1301	$\|\Psi_{w_3,2R}\rangle$ 1363	$\|\Psi_{1z,2R}\rangle$ 1615
$\langle\Phi_{1z}\|$	0.52	0.12	0.02	0.10	0.01	0.02
$\langle\Phi_{1R,w_3}\|$	0.21	0.53	0.02	0.00	0.03	0.01
$\langle\Phi_{1z,1R}\|$	0.00	0.03	0.43	0.12	0.06	0.04
$\langle\Phi_{bu}\|$	0.11	0.03	0.13	0.27	0.09	0.01
$\langle\Phi_{w_3,2R}\|$	0.00	0.00	0.11	0.11	0.23	0.01
$\langle\Phi_{1z,2R}\|$	0.00	0.00	0.00	0.02	0.00	0.32

3. $H(D_2O)_2^+$

Figure 4 shows the computed MCTDH spectrum of $H(D_2O)_2^+$ in the range of 700–1700 cm^{-1} together with the experimental spectrum measured using Ar as the tagging agent.[16] The experimental spectrum presents two major peaks at about 750 and 930 cm^{-1} which correspond to two possible situations, either D is found in the central position or H is found in the central position. Hence the experimental spectrum in Fig. 4 corresponds to the superposition of two different spectra. From the point of view of the assignment

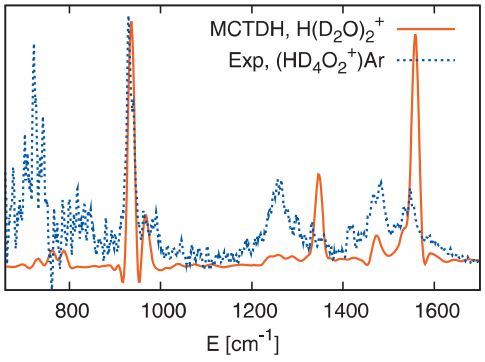

FIG. 4. For $H(D_2O)_2^+$ comparison of the computed MCTDH IR spectrum (full line) with an experimental spectrum of $HD_4O_2^+$ measured using Ar as the messenger atom (dotted line) (Ref. 16). The experimental spectrum is a statistical mixture of the spectrum corresponding to H in the central position and of the spectrum corresponding to H in an external position (Ref. 16).

of spectral lines and of correlation, this is the most complex of all considered spectra. Figure 1(c) presents the MCTDH spectrum with assignments in the spectral range of 0–4000 cm^{-1}. Table VI presents the $|\langle\Phi_l|\Psi_m\rangle|^2$ matrix elements for the $H(D_2O)_2^+$ case. Here the deuteration of the external positions brings the position of the zeroth-order state $|\Phi_{bu}\rangle$ down to lower frequencies by about 300 cm^{-1}, while the zeroth-order states $|\Phi_{1z}\rangle$ and $|\Phi_{1z,1R}\rangle$ remain almost unaffected. This results in a situation in which the zeroth-order $|\Phi_{bu}\rangle$ is found between $|\Phi_{1z}\rangle$ and $|\Phi_{1z,1R}\rangle$. State $|\Phi_{w_3,2R}\rangle$ is also found in this energy region. These four zeroth-order states strongly couple to each other and are responsible for the three peaks at 936, 1347, and 1559 cm^{-1}. By inspecting the $|\langle\Phi_l|\Psi_m\rangle|^2$ matrix elements in Table VI it is seen that the 4×4 block corresponding to $(1z)$, $(w_3,2R)$, (bu), and $(1z,1R)$ excitations has important nondiagonal elements. The peak at 936 cm^{-1}, assigned as $(\widetilde{1z})$, has almost equal relative contribution from $|\Phi_{1z}\rangle$ and $|\Phi_{bu}\rangle$. The central peak at 1347 cm^{-1} assigned as (bu) has as leading contribution $|\Phi_{w_3,2R}\rangle$ and almost equal participation from $|\Phi_{bu}\rangle$ and $|\Phi_{1z}\rangle$, while the peak at 1564 cm^{-1} is a mixture of $|\Phi_{bu}\rangle$ and $|\Phi_{1z,1R}\rangle$ with a larger participation of the latest. An eigenstate of energy of 1245 cm^{-1} presents a very low absorption in the IR spectrum. This state has as leading contribution $|\Phi_{w_3,2R}\rangle$ and important and almost equal participation of $|\Phi_{1z}\rangle$, $|\Phi_{bu}\rangle$, and $|\Phi_{1z,1R}\rangle$. The strong couplings shaping the middle spectral region of the spectrum of $H(D_2O)_2^+$ are reflected in a matrix of $|\langle\Phi_l|\Psi_m\rangle|^2$ elements that is less diagonally dominant than in the previously discussed cases. Assignments of the eigenstates with energies of 936 and 1347 cm^{-1} are a bit arbitrary because of the strong mixing and the fact that a single leading contribution cannot be clearly identified. Therefore these eigenstates are denoted with a tilde in both Table VI and Fig. 1(c). The eigenstate with energy of 1245 cm^{-1} has not been signaled by a tilde. This eigenstate presents contributions from four zeroth-order states, but one of them, $|\Phi_{w_3,2R}\rangle$ can be clearly identified as the leading contribution. The $(w_3,1R)$ peak is of reduced intensity due to its redshift and consequent decoupling from the zeroth-order $(1z)$. The $(1z,2R)$ state is located far from peaks from which it can borrow intensity and shows no IR absorption.

TABLE VI. For $H(D_2O)_2^+$, matrix elements $|\langle\Phi_l|\Psi_m\rangle|^2$, where $|\Phi_l\rangle$ is a zeroth-order state and $|\Psi_m\rangle$ is an eigenstate. The naming of each eigenstate $|\Psi_m\rangle$ is based on the leading contribution of the zeroth-order states $|\Phi_l\rangle$. The assignment of eigenstates marked with a tilde is a bit arbitrary due to the strong underlying mixing of zeroth-order states.

$H(D_2O)_2^+$ Energy (cm^{-1})	$\|\Psi_{w_3,1R}\rangle$ 760	$\|\tilde{\Psi}_{1z}\rangle$ 936	$\|\Psi_{w_3,2R}\rangle$ 1245	$\|\tilde{\Psi}_{bu}\rangle$ 1347	$\|\Psi_{1z,1R}\rangle$ 1559	$\|\Psi_{1z,2R}\rangle$ 2056
$\langle\Phi_{1R,w_3}\|$	0.65	0.06	0.00	0.00	0.00	0.00
$\langle\Phi_{1z}\|$	0.05	0.28	0.11	0.16	0.09	0.02
$\langle\Phi_{w_3,2R}\|$	0.00	0.00	0.36	0.26	0.02	0.00
$\langle\Phi_{bu}\|$	0.02	0.31	0.14	0.19	0.15	0.00
$\langle\Phi_{1z,1R}\|$	0.00	0.01	0.14	0.02	0.33	0.04
$\langle\Phi_{1z,2R}\|$	0.00	0.00	0.00	0.01	0.00	0.16

TABLE VII. For $D(H_2O)_2^+$, matrix elements $|\langle\Phi_l|\Psi_m\rangle|^2$, where $|\Phi_l\rangle$ is a zeroth-order state and $|\Psi_m\rangle$ is an eigenstate. The naming of each eigenstate $|\Psi_m\rangle$ is based on the leading contribution of the zeroth-order states $|\Phi_l\rangle$.

$D(H_2O)_2^+$ Energy (cm^{-1})	$\|\Psi_{1z}\rangle$ 729	$\|\Psi_{w_3,1R}\rangle$ 943	$\|\Psi_{1z,1R}\rangle$ 1214	$\|\Psi_{w_3,2R}\rangle$ 1486	$\|\Psi_{bu}\rangle$ 1660	$\|\Psi_{1z,2R}\rangle$ 1704
$\langle\Phi_{1z}\|$	0.63	0.04	0.05	0.01	0.03	0.05
$\langle\Phi_{1R,w_3}\|$	0.05	0.64	0.04	0.00	0.03	0.00
$\langle\Phi_{1z,1R}\|$	0.00	0.05	0.56	0.00	0.02	0.00
$\langle\Phi_{w_3,2R}\|$	0.00	0.00	0.06	0.33	0.06	0.02
$\langle\Phi_{bu}\|$	0.06	0.00	0.02	0.00	0.51	0.20
$\langle\Phi_{1z,2R}\|$	0.00	0.00	0.00	0.00	0.10	0.37

4. $D(H_2O)_2^+$

In contrast to $H(D_2O)_2^+$, deuteration of the central position alone in $D(H_2O)_2^+$ leads to the simplest and most diagonal dominant IR spectrum of this series, shown in Fig. 1(d). Here the zeroth-order $(1z)$ state shifts to lower frequencies and decouples from $(1R,w_3)$. The peak at 785 cm^{-1} is cleanly assigned to $(1z)$. $(1z)$ decouples as well from (bu). This brings the position of the (bu) peak down to 1662 cm^{-1}, closer to the bending frequency of an isolated water molecule and explains the reduced intensity. Note that the position of (bu) at 1758 cm^{-1} in $H(H_2O)_2^+$ was due to strong coupling with the central proton $(1z)$ mode. Due to the isotopic substitution the $(1z,2R)$ peak is shifted down, ending relatively close to (bu). The doublet formed by (bu) and $(1z,2R)$ is the only structure related to a resonance in $D(H_2O)_2^+$. However, both lines can be cleanly assigned, as seen by inspecting the contribution of the corresponding zeroth-order states in Table VII.

IV. SUMMARY AND CONCLUSION

The IR spectra and low lying vibrational eigenstates of $H(H_2O)_2^+$, $D(D_2O)_2^+$, $H(D_2O)_2^+$, and $D(H_2O)_2^+$ are computed by quantum dynamics in full dimensionality using the MCTDH method on an accurate PES. The ZPE is computed for the four isotopologues by improved relaxation and an excellent agreement with the reference diffusion Monte Carlo results is found in all cases. The first ten vibrational eigenstates, which are related to the wagging and internal rotation coordinates, are computed by BIR. The eigenener-

gies of the wagging vibrational states present important shifts to lower frequencies upon deuterium substitution in the external positions but are almost independent of the isotope substitution in the central position. The only exception is the (w_3) state. This is a two-quanta wagging state in which one water molecule is preferentially in planar conformation while the other one is pyramidalized and vice versa. This state has the correct symmetry to couple to the asymmetric excitation of the central proton $(1z)$, and its energy varies in the order of 10 cm^{-1} up or down depending on the isotope substitution in the central position.

The IR spectra of the four considered isotopologues are computed and assigned. These spectra are depicted in Fig. 1. The middle spectral region between 600 and 2000 cm^{-1} is strongly dependent on the isotopic substitution of the cation. Not only the expected line shifts take place, but important changes in the intensities of the lines occur as well. The assignment of the four spectra ravels that couplings and Fermi resonances responsible for their shape are strongly dependent on isotope substitution. The assignments are performed according to the products $|\langle\Phi_l|\Psi_m\rangle|^2$, which tell to which extent a particular and well defined zeroth-order vibration $|\Phi_l\rangle$ participates in the eigenstate $|\Psi_m\rangle$ responsible for a particular spectral line. The IR spectrum of $H(H_2O)_2^+$ features a doublet peak centered at 1000 cm^{-1}, which originates from a Fermi resonance of zeroth-order states $|\Phi_{w_3,1R}\rangle$ and $|\Phi_{1z}\rangle$. A block of three zeroth-order states with nonnegligible couplings between them, $|\Phi_{1z,1R}\rangle$, $|\Phi_{w_3,2R}\rangle$, and $|\Phi_{bu}\rangle$, is responsible for the next two peaks at 1392 and 1756 cm^{-1}. The leading contributions to the two eigenstates are $(1z,1R)$ and (bu), respectively. However, $(w_3,2R)$ has an almost equal contribution to the first peak as $(1z,1R)$. Next the IR spectrum of $D(D_2O)_2^+$ is assigned. This spectrum features a doublet with peaks at 683 and 813 cm^{-1}. The two leading contributions to the two peaks are the two coupled $|\Phi_{1z}\rangle$ and $|\Phi_{w_3,1R}\rangle$ zeroth-order states, respectively. Hence $D(D_2O)_2^+$ features a Fermi resonance similar to the one in $H(H_2O)_2^+$ but with the two peaks at lower frequencies and in reverse order. The zeroth-order states $|\Phi_{1z,1R}\rangle$, $|\Phi_{w_3,2R}\rangle$, and $|\Phi_{bu}\rangle$ form also a block of three coupled states in this case. The two peaks at 1301 and 1363 cm^{-1} are related to a Fermi resonance between zeroth-order states $|\Phi_{bu}\rangle$ and $|\Phi_{w_3,2R}\rangle$, respectively. The most complex spectrum of the series is $H(D_2O)_2^+$. Here the isotopic substitution in the external positions shifts the zeroth-order excitations $(w_3,1R)$, $(w_3,2R)$, and (bu) down to lower frequencies, while $(1z)$ and $(1z,1R)$ remain mostly unaffected. In this case $(w_3,1R)$ uncouples from $(1z)$ and a block of four zeroth-order states with important couplings among them, namely, $|\Phi_{1z}\rangle$, $|\Phi_{w_3,2R}\rangle$, $|\Phi_{bu}\rangle$, and $|\Phi_{1z,1R}\rangle$, is responsible for the three peaks at 936, 1347, and 1559 cm^{-1}. It is not possible to identify a clear leading contribution to the peak at 936 cm^{-1}, which is mostly a mixture of $(1z)$ and (bu), neither for the peak at 1347 cm^{-1}, which is a mixture of $(1z)$, $(w_3,2R)$, and (bu). The simplest of all spectra is $D(H_2O)_2^+$. Here the increase in mass in the central position shifts the zeroth-order $(1z)$ excitation to a lower frequency, so that it separates from other zeroth-order excitations. The coupling between zeroth-order states is in this case much smaller than in other cases, as seen by inspecting Table VII, which is clearly diagonal dominant.

In this contribution we provide an in-depth theoretical analysis of the IR spectroscopy of four isotopologues of the Zundel cation. The dramatic differences between the spectra of these isotopologues are indicative of the complex underlying dynamics, with couplings and Fermi resonances being strongly dependent on the masses of the atoms. These results contribute to the general understanding of the complex dynamics of protonated water clusters and the hydrated proton.

ACKNOWLEDGMENTS

The authors thank Professor J. Bowman for providing the potential-energy routine, M. Brill for help with the parallel version of MCTDH, and the Scientific Supercomputing Center Karlsruhe for generously providing computer time. Financial support by the Deutsche Forschungsgemeinschaft (DFG) is also gratefully acknowledged. O.V. is grateful to the European Union for financial support through the Marie-Curie Program.

[1] D. Marx, M. Tuckerman, J. Hutter, and M. Parrinello, Nature (London) **397**, 601 (1999).
[2] J. M. Headrick, E. G. Diken, R. S. Walters, N. I. Hammer, R. A. Christie, J. Cui, E. M. Myshakin, M. A. Duncan, M. A. Johnson, and K. D. Jordan, Science **308**, 1765 (2005).
[3] R. Pomes and B. Roux, Biophys. J. **82**, 2304 (2002).
[4] G. Mathias and D. Marx, Proc. Natl. Acad. Sci. U.S.A. **104**, 6980 (2007).
[5] O. F. Mohammed, D. Pines, J. Dreyer, E. Pines, and E. T. J. Nibbering, Science **310**, 83 (2005).
[6] S. Woutersen and H. J. Bakker, Phys. Rev. Lett. **96**, 138305 (2006).
[7] A. Chandra, M. E. Tuckerman, and D. Marx, Phys. Rev. Lett. **99**, 145901 (2007).
[8] D. J. Mann and M. D. Halls, Phys. Rev. Lett. **90**, 195503 (2003).
[9] R. J. Mashl, S. Joseph, N. R. Aluru, and E. Jakobsson, Nano Lett. **3**, 589 (2003).
[10] O. Vendrell and H.-D. Meyer, J. Chem. Phys. **122**, 104505 (2005).
[11] J.-W. Shin, N. I. Hammer, E. G. Diken, M. A. Johnson, R. S. Walters, T. D. Jaeger, M. A. Duncan, R. A. Christie, and K. D. Jordan, Science **304**, 1137 (2004).
[12] K. R. Asmis, N. L. Pivonka, G. Santambrogio, M. Brummer, C. Kaposta, D. M. Neumark, and L. Woste, Science **299**, 1375 (2003).
[13] T. D. Fridgen, T. B. McMahon, L. MacAleese, J. Lemaire, and P. Maitre, J. Phys. Chem. A **108**, 9008 (2004).
[14] J. M. Headrick, J. C. Bopp, and M. A. Johnson, J. Chem. Phys. **121**, 11523 (2004).
[15] N. I. Hammer, E. G. Diken, J. R. Roscioli, M. A. Johnson, E. M. Myshakin, K. D. Jordan, A. B. McCoy, J. M. Bowman, and S. Carter, J. Chem. Phys. **122**, 244301 (2005).
[16] L. McCunn, J. Roscioli, M. Johnson, and A. McCoy, J. Phys. Chem. B **112**, 321 (2008).
[17] L. R. McCunn, J. R. Roscioli, B. M. Elliott, M. A. Johnson, and A. B. McCoy, J. Phys. Chem. A **112**, 6074 (2008).
[18] M. V. Vener, O. Kühn, and J. Sauer, J. Chem. Phys. **114**, 240 (2001).
[19] J. Dai, Z. Bacic, X. C. Huang, S. Carter, and J. M. Bowman, J. Chem. Phys. **119**, 6571 (2003).
[20] X. Huang, B. J. Braams, and J. M. Bowman, J. Chem. Phys. **122**, 044308 (2005).
[21] A. B. McCoy, X. Huang, S. Carter, M. Y. Landeweer, and J. M. Bowman, J. Chem. Phys. **122**, 061101 (2005).
[22] J. Sauer and J. Dobler, ChemPhysChem **6**, 1706 (2005).
[23] M. Kaledin, A. L. Kaledin, and J. M. Bowman, J. Phys. Chem. A **110**, 2933 (2006).
[24] O. Vendrell, F. Gatti, and H.-D. Meyer, Angew. Chem., Int. Ed. **46**, 6918 (2007).
[25] O. Vendrell, F. Gatti, D. Lauvergnat, and H.-D. Meyer, J. Chem. Phys. **127**, 184302 (2007).

[26] O. Vendrell, F. Gatti, and H.-D. Meyer, J. Chem. Phys. **127**, 184303 (2007).
[27] O. Vendrell and H.-D. Meyer, Phys. Chem. Chem. Phys. **10**, 4692 (2008).
[28] O. Vendrell, F. Gatti, and H.-D. Meyer, Angew. Chem., Int. Ed. **48**, 352 (2009).
[29] O. Vendrell, M. Brill, F. Gatti, D. Lauvergnat, and H.-D. Meyer, J. Chem. Phys. **130**, 234305 (2009).
[30] M. Kaledin, A. L. Kaledin, J. M. Bowman, J. Ding, and K. D. Jordan, J. Phys. Chem. A **113**, 7671 (2009).
[31] U. Manthe, H.-D. Meyer, and L. S. Cederbaum, J. Chem. Phys. **97**, 3199 (1992).
[32] M. H. Beck, A. Jäckle, G. A. Worth, and H.-D. Meyer, Phys. Rep. **324**, 1 (2000).
[33] H.-D. Meyer and G. A. Worth, Theor. Chem. Acc. **109**, 251 (2003).
[34] H.-D. Meyer, G. A. Worth, M. H. Beck, A. Jäckle, U. Manthe, M. Ehara, A. Raab, M.-C. Heitz, S. Sukiasyan, C. Cattarius, S. Wefing, F. Gatti, M. Nest, F. Otto, A. Markmann, M. R. Brill, and O. Vendrell, The MCTDH Package, version 8.4, http://mctdh.uni-hd.de/, 2007.
[35] S. Carter, S. J. Culik, and J. M. Bowman, J. Chem. Phys. **107**, 10458 (1997).
[36] J. M. Bowman, S. Carter, and X. Huang, Int. Rev. Phys. Chem. **22**, 533 (2003).
[37] H. Rabitz and O. F. Alis, J. Math. Chem. **25**, 197 (1999).
[38] A. Jäckle and H.-D. Meyer, J. Chem. Phys. **104**, 7974 (1996).
[39] A. Jäckle and H.-D. Meyer, J. Chem. Phys. **109**, 3772 (1998).
[40] H.-D. Meyer, F. Le Quéré, C. Léonard, and F. Gatti, Chem. Phys. **329**, 179 (2006).
[41] L. J. Doriol, F. Gatti, C. Iung, and H.-D. Meyer, J. Chem. Phys. **129**, 224109 (2008).